
Beyond Pixel Histories: World Models with Persistent 3D State

Samuel Garcin^{*1} Thomas Walker^{*1} Steven McDonagh¹ Tim Pearce² Hakan Bilen¹ Tianyu He²
Kaixin Wang² Jiang Bian²

francelico.github.io/persist.github.io

Abstract

Interactive world models continually generate video by responding to a user’s actions, enabling open-ended generation capabilities. However, existing models typically lack a 3D representation of the environment, meaning 3D consistency must be implicitly learned from data, and spatial memory is restricted to limited temporal context windows. This results in an unrealistic user experience and presents significant obstacles to downstream tasks such as training agents. To address this, we present PERSIST, a new paradigm of world model which simulates the evolution of a latent 3D scene: **environment**, **camera**, and **renderer**. This allows us to synthesize new frames with persistent spatial memory and consistent geometry. Both quantitative metrics and a qualitative user study show substantial improvements in spatial memory, 3D consistency, and long-horizon stability over existing methods, enabling coherent, evolving 3D worlds. We further demonstrate novel capabilities, including synthesising diverse 3D environments from a single image, as well as enabling fine-grained, geometry-aware control over generated experiences by supporting environment editing and specification directly in 3D space.

1. Introduction

Interactive world models aim to generate experiences that unfold over time in response to user actions, enabling a new class of photo-realistic, personalised, and immersive interactive experiences for human users (Kanervisto et al., 2025; Ball et al., 2025; Huang et al., 2025b). At the same time, such models hold significant potential for safely training embodied agents within simulators learned directly from

data (Hafner et al., 2025; Micheli et al., 2023; Alonso et al., 2024; Garcin et al., 2024). Unlike passive video generation, interactive generation requires models to respond meaningfully to external interventions. In this setting, realism is not determined solely by per-frame visual quality, but by the degree to which the generated experience maintains persistent environments and stable dynamics throughout extended rollouts.

Most existing approaches to interactive video generation rely on auto-regressive (AR) models that condition on the history of past observations and actions to generate the most recent frame, often using diffusion-based transformers with causal attention (Peebles & Xie, 2023). This formulation is attractive: it naturally supports real-time action conditioning, allows generation to proceed indefinitely, and integrates cleanly with recent advances in large-scale video modelling. As a result, AR video diffusion models form the backbone of many recent neural game engines and interactive world models (Che et al., 2024; He et al., 2025; Valevski et al., 2024b; Zhang et al., 2025; Yu et al., 2025).

However, conditioning on high-dimensional visual observations is computationally expensive, and the number of prior frames that AR models can ingest is tightly constrained by hardware. In practice, this limits AR generation to condition on what amounts to only a few seconds of past footage, even when observations are compressed to lower spatial and/or temporal resolutions using learned autoencoders. As a result, a growing body of work has explored how best to populate this limited contextual window, most commonly through heuristic strategies that retrieve individual key frames from a memory bank of past observations (Xiao et al., 2025a; Huang et al., 2025a).

Yet, an inherent flaw of key-frame retrieval methods is that each pixel observation provides only partial, highly redundant, and viewpoint-dependent information about the world at a fixed point in time. As the memory bank grows, identifying the relevant past evidence becomes increasingly difficult. As a result, generating extended and coherent experiences within complex 3D environments remains an open challenge

^{*}Equal contribution ¹University of Edinburgh ²Microsoft Research. Correspondence to: Samuel Garcin <s.garcin@ed.ac.uk>, Kaixin Wang <kaixin96.wang@gmail.com>.

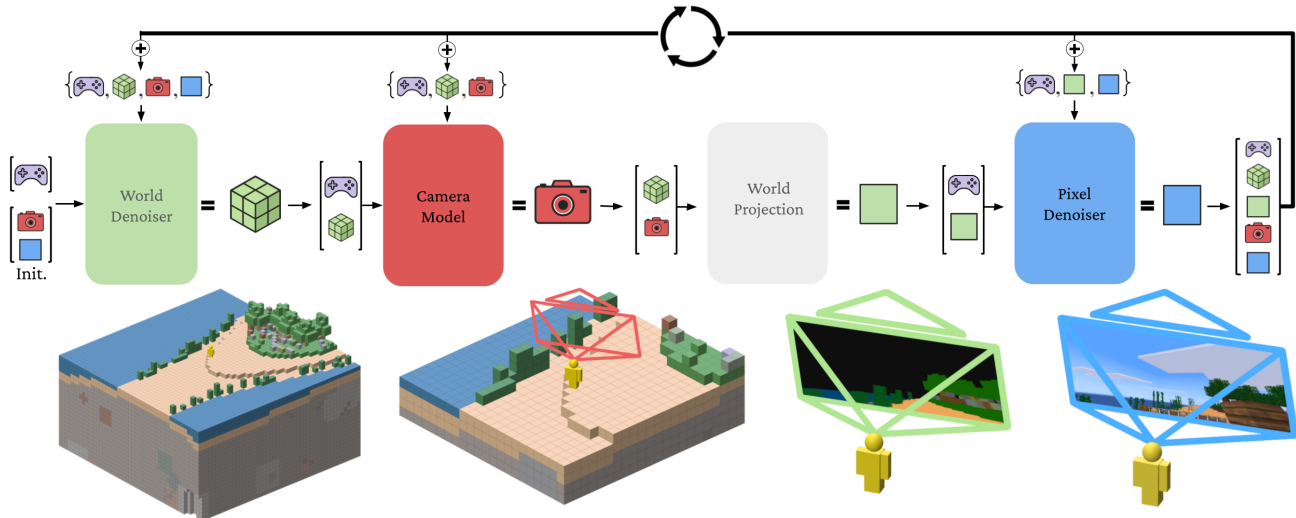


Figure 1. Initialized with a single pixel frame, PERSIST evolves in an auto-regressive loop in response to user actions (🎮). We first denoise the 3D environment centred on the agent in the form of a latent *world-frame* (🟩). Next, camera parameters (📷) are predicted with a feed-forward transformer. We then project the world to the camera plane to form a depth-ordered stack of world latents (🟩). Finally, pixel latents (🟦) are denoised, using pixel-aligned 3D information from the world latents stack (🟩) as guidance.

even for frontier models.¹

In this work, we propose to depart from pixel-based histories and substitute key frame retrieval with *active key frame generation*. We are inspired by traditional 3D simulators and game engines, which maintain coherence by directly rendering pixel frames from a persistent and dynamically evolving 3D state of the world. We introduce PERSIST, a framework that brings persistence to learned AR world models by tracking a dynamic 3D representation of the environment. We describe our framework in Figure 1. PERSIST decomposes world simulation into three coupled components: a *world-frame model* that predicts how a learned representation of a 3D scene evolves over time, a *camera model* that tracks the agent’s viewpoint within this scene, and a *world-to-pixel generation module* that produces observations via differentiable projection and a learned rendering function.

Rather than treating pixels as the primary carrier of memory, PERSIST models the structure and dynamics of the environment in a latent 3D space. This persistent world representation captures how the scene evolves over time, while the camera acts as a query mechanism that extracts the subset of 3D information relevant to guide the generation of the current frame. This formulation enables long-horizon rollouts with fixed-cost memory, enforces geometric consistency by construction, and remains fully learned and compatible with modern diffusion and flow-based training objectives.

¹Closed-source frontier models report achieving up to one minute of visual memory, representing the current frontier of AR generation (Ball et al., 2025).

We evaluate PERSIST in a complex 3D environment and find that explicitly modelling persistent 3D dynamics leads to substantially improved long-horizon generation quality compared to rolling-window and memory-retrieval baselines. Our approach exhibits stronger temporal stability, improved spatial memory when revisiting previously observed regions, and markedly better 3D consistency overall. Beyond quantitative gains, persistent world representation enables new capabilities, including explicit 3D scene initialisation, mid-episode scene edits, and the emergence of off-screen dynamic processes that continue to evolve even when not directly observed.

2. Related Works

World models. World models (Ha & Schmidhuber, 2018) aim to simulate environments by predicting future states conditioned on user actions. Recent progress in video generation models enable high-fidelity interactive simulation (Ball et al., 2025; Alonso et al., 2024; Decart et al., 2024). However, maintaining spatial and temporal consistency over extended rollouts remains challenging due to the finite number of past frames existing models can incorporate as context. Prior works propose to alleviate this limitation via spatio-temporal compression of input tokens (Hafner et al., 2025), memory-efficient attention mechanisms (Po et al., 2025) or by populating the model context window with frames sampled from the full generation history (Song et al., 2025). Among this latter class of approaches, (Xiao et al., 2025a; Huang et al., 2025a) propose sampling strategies that retrieve key-frames according to their spatial relevance.

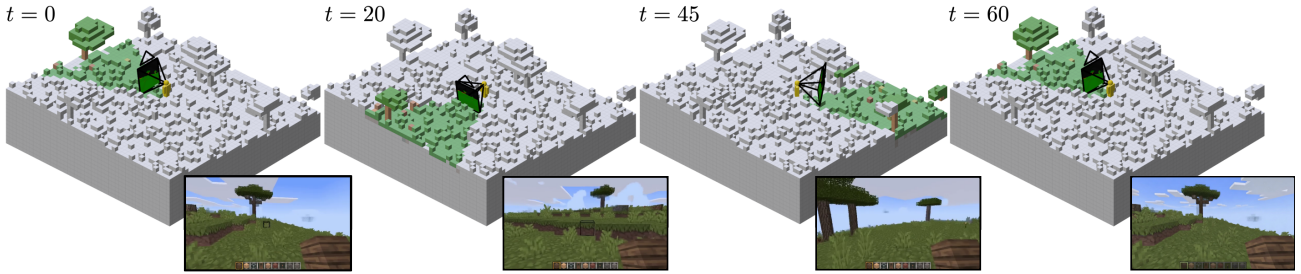


Figure 2. PERSIST enables long-horizon spatial memory by modelling the dynamics of a 3D world-frame around the agent. Camera parameters then act as memory look-up key, fetching relevant features from the world frame via a geometric projection (here visualized as the coloured voxels).

Nevertheless, such methods rely on retrieving relevant information from an ever-growing history of pixel observations, a task that becomes increasingly difficult and costly over extended rollouts. In contrast, PERSIST retrieves contextual information directly from a dynamically evolving 3D latent state, making its information retrieval mechanism independent of episode length.

3D environment representations. In parallel, a growing number of approaches incorporate explicit 3D representations into their generative architectures to produce explorable and spatially consistent environments (Huang et al., 2025b; Labs, 2025; Zhou et al., 2025). However, these environments remain static, restricting interaction to basic navigation within a frozen world. In contrast, PERSIST learns a 3D representation that evolves over time, enabling it to capture dynamic processes occurring within the environment, and richer agent–environment interactions.

Neural rendering. While neural radiance fields (NeRFs) have become a popular, compact, and resolution-free representation of 3D scenes (Mildenhall et al., 2021; Müller et al., 2022; Li et al., 2023), they rely on costly ray marching with many neural network queries, making them prohibitively expensive for interactive use. PERSIST instead takes inspiration from neural deferred shading, which rasterizes explicit geometry into screen-space features and decodes them with learned neural shaders, enabling more efficient rendering (Thies et al., 2019; Worchel et al., 2022; Walker et al., 2023; Chen et al., 2023; Deering et al., 1988).

3. Preliminaries

Rectified flow matching. Our approach is based on the paradigm of flow matching and diffusion models (Lipman et al., 2023), where the task is to restore a clean data sample x^0 given a noised version x^τ . The noise level $\tau \in [0, 1]$ determines the degree of corruption of the data, where $\tau = 0$ denotes clean data and $\tau = 1$ indicates pure noise. Rectified flow models (Lipman et al., 2023; Albergo & Vanden-Eijnden, 2023) employ a noising process $x^\tau = (1 - \tau)x^0 + \tau x^1$ that linearly interpolates be-

tween sample x^0 and noise $x^1 \sim \mathcal{N}(0, \mathbb{I})$. Provided with a noised sample and corresponding noise level, the model \mathcal{V}_θ is trained to predict the velocity vector $v = x^0 - x^1$ pointing towards the clean data via the conditional flow matching objective (CFM) (Lipman et al., 2023):

$$\mathcal{L}(\theta) = \left\| \mathcal{V}_\theta(x^\tau, \tau) - (x^0 - x^1) \right\|^2 \quad \tau \sim p(\tau), \quad (1)$$

where τ is often sampled from a uniform or logit-normal distribution. During inference, random noise x^1 is iteratively denoised into a clean sample x^0 over K sampling steps, with uniform or variable step size d^k :

$$x^{\tau-d^k} = x^\tau + \mathcal{V}_\theta(x^\tau, \tau)d^k, \quad \tau \leftarrow \tau - d^k. \quad (2)$$

Autoregressive video generation. While full-sequence video diffusion models treat videos as a single data sample to be denoised jointly at inference time, AR models treat videos as a sequence of individual frames $X_1^n = x_1, x_2, \dots, x_n$ to be diffused sequentially.² AR models employ causal masking strategies during training to ensure no information travels from the future into the past. Diffusion forcing (Chen et al., 2024) improves the generation stability of AR video diffusion models at inference by introducing per-frame noise levels that are sampled independently during training. At inference, AR generation becomes a special case of the training setup, where the current frame is iteratively denoised from random noise and past frames receive a small fixed noise level τ_{ctx} .

Interactive world simulation. Because generation proceeds step-by-step, AR models can in principle be unrolled indefinitely and conditioned on external control signals provided at each timestep. This enables a transition from passive video generation to interactive world simulation. We employ a similar formalism as Valevski et al. (2024a) to characterize the problem of learning a *world model*, which

²Notation-wise, the noise level of an individual frame x_t^τ is indicated by superscript τ , its position in the sequence by subscript t . In the case of a truncated sequence X_k^t , we overload the notation to have k and t indicate its beginning and end.

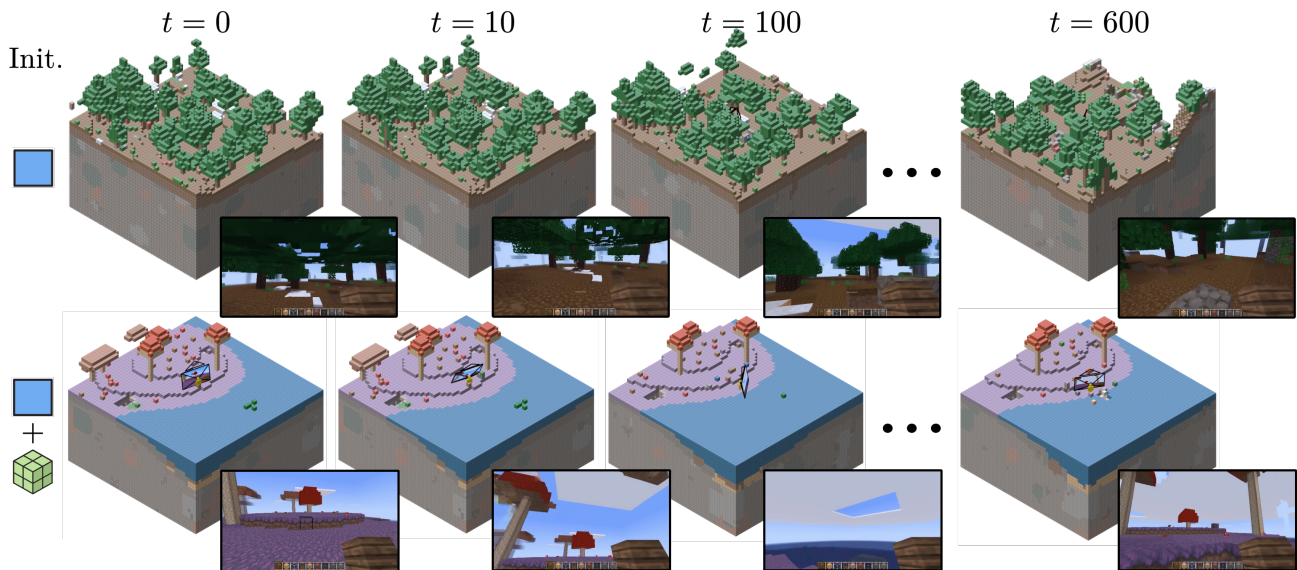


Figure 3. PERSIST can be initialized with a single RGB frame (■, row 1), or with a single RGB and world frame (■ + ■, row 2). We visualize the world-frames and videos produced by an auto-regressive rollout of 600 timesteps. Even with a single RGB frame for initialization, PERSIST can generate cohesive and evolving worlds.

we define here as a learned simulator of some *interactive environment* \mathcal{E} :

$$\mathcal{E} = \langle \mathbb{S}, \mathbb{O}, \mathbb{A}, \Omega, p \rangle, \quad (3)$$

where \mathbb{S} is the space of latent states, \mathbb{O} the space of observations, \mathbb{A} the set of actions that may be taken within the environment, $\Omega : \mathbb{S} \rightarrow \mathbb{O}$ a partial projection function mapping states to observations, $p(s'|a, s)$ is a transition probability function such that $s, s' \in \mathbb{S} \times \mathbb{S}$ and $a \in \mathbb{A}$. Given a distribution of initial states p_0 and episode length N_0 , a policy π in charge of selecting actions in \mathcal{E} , and a distance metric between observation sequences $D : \mathbb{O}^n \times \mathbb{O}^n \rightarrow \mathbb{R}$, learning an interactive world simulation of \mathcal{E} consists of minimising the objective $\mathbb{E}[D(O^n, \tilde{O}^n)]$. O^n is a sequence of observations of length $n \sim N_0$ collected in \mathcal{E} from starting state $s_0 \sim p_0$ and by following π ; and \tilde{O}^n is obtained from an AR model Q_θ initialised at $\mathbf{o}_0 = \Omega(s_0)$ and subjected to the same action sequence.

4. A Persistent Environment Representation

Learning an auto-regressive model Q_θ is often challenging when \mathcal{E} is a complex 3D environment featuring high dimensional pixel observations. First, memory constraints limit Q_θ to condition on a finite context window of past K frames, which degrades temporal consistency once the generated episode exceeds this horizon. Second, pixel observations typically provide partial information about the environment’s hidden state, making learning accurate transition dynamics challenging. One might therefore attempt to have Q_θ condition on some approximation of the hidden

state s ; however s can be arbitrarily complex or entirely unmeasurable. Even if s was accessible, learning the observation function $\Omega : \mathbb{S} \rightarrow \mathbb{O}$ to recover observations can be a comparably challenging problem. For example, in the case of a video game, s would be the program’s dynamic memory contents, which may not be particularly helpful for easily recovering pixel observations.

Instead, we define a proxy $\tilde{s} = \langle \mathbf{w}, \mathbf{c} \rangle$, where \mathbf{w} is a *world-frame* representing a fixed region of space centred on the agent, and \mathbf{c} is a camera state encoding the agent’s view within \mathbf{w} . Although not a perfect replacement for the true hidden state, \tilde{s} is an effective modelling choice when \mathcal{E} is a 3D environment, as it lets us:

1. **Simplify information retrieval.** Figure 2 demonstrate how the world-frame \mathbf{w}_t can function as a dynamic *spatial memory* module throughout the episode, while the camera state \mathbf{c}_t acts as a *spatial lookup-key* to retrieve the spatial information in \mathbf{w}_t that is necessary to reconstruct \mathbf{o}_t . \mathbf{c}_t encodes the information to project this information to screen-space, without requiring explicit knowledge of the true observation function.
2. **Improve dynamics predictions.** Tracking \mathbf{w} and \mathbf{c} over time facilitates modelling dynamics that are difficult to infer from pixel observations alone, such as interactions or collisions with out-of-view objects, or tracking how occluded regions of the environment change over time.

5. PERSIST

We present PERSIST (Persistent Environment Representations for Simulating Interactive Space-Time), a world simulation framework for complex 3D environments. PERSIST decomposes the world simulation objective into the tasks of *world frame prediction*, *camera prediction* and *world-to-pixel generation*.

Dataset construction and pre-processing. The different components of PERSIST are trained from a dataset of trajectories collected from \mathcal{E} . A trajectory consists of a sequence of pixel observations O , actions A , world-frames W and camera views C . In this work, we assume that W and C are directly obtainable from \mathcal{E} , the former as a 3D voxel grid within a cuboid centered on the agent, and the latter as a vector encoding the camera intrinsics and extrinsics. Actions are embedded as a 23-dimensional multi-hot encoding of key presses and discretised mouse movements. We train a 2D-VAE and a 3D-VAE to encode pixel- and world-frames into latent patches \bar{o} and \bar{w} of 10×10 pixels and 4^3 voxels respectively.

5.1. World-Frame and Camera Prediction

World frame prediction. At each timestep, a new world-frame is generated by sampling

$$\bar{w}_t \sim \mathcal{W}_\theta(\bar{w}_t | \bar{W}_{t-K}^{t-1}, A_{t-K}^t, C_{t-K-1}^{t-1}, \bar{O}_{t-K-1}^{t-1}), \quad (4)$$

where K is the model’s temporal context window and latents \bar{W}_{t-K}^{t-1} and \bar{O}_{t-K-1}^{t-1} are encoded using the VAEs. \mathcal{W}_θ is parametrised as a rectified flow model with a causal Diffusion Transformer (DiT) backbone (Peebles & Xie, 2023) employing interleaved spatial, temporal and cross-attention modules (Decart et al., 2024). We modify the spatial module to handle three spatial dimensions, and replace RoPE spatial embeddings (Su et al., 2024) with absolute position embeddings of the XYZ coordinates of the centroid of each voxel token. We keep the temporal module as-is. Actions and cameras are jointly embedded using a multi-layer perceptron (MLP). The resulting embeddings are added to the denoising timestep embedding and injected into each module via Adaptive Layer Normalisation (AdaLN) (Peebles & Xie, 2023). We employ Plücker embeddings (Xiao et al., 2025a; Sitzmann et al., 2021) to convey information on how individual pixel patches project to 3D space. These embeddings are computed from C_{t-K-1}^{t-1} and are concatenated channel-wise to the pixel patches. The resulting patches are then injected into the model via the cross-attention module. Finally, we employ the 3D-VAE to decode \bar{w}_t to its native resolution.

Crucially, \mathcal{W}_θ supports conditioning on $\bar{W} = \emptyset$, making it able of generating an initial world frame w_0 from initial condition $\langle o_0, c_0 \rangle$ at inference time. Thus, while we rely on W to train \mathcal{W}_θ , we do not have to rely on ground truth

3D conditioning during inference. We provide examples for each inference configuration in Figure 3.

Camera model. At any given timestep, cameras are represented as the 10-dimensional vector $c = \langle \text{pos}, \text{rot}, \text{fov} \rangle$, where $\text{pos} \in \mathbb{R}^3$ encodes the camera’s position in the world-frame, $\text{rot} \in \mathbb{R}^6$ its orientation as a 6D continuous rotation (Zhou et al., 2019), and $\text{fov} \in \mathbb{R}$ its field-of-view. The camera model predicts $c_t = \mathcal{C}_\theta(C_{t-1-K}^{t-1}, W_{t-K}^t, A_{t-K}^t)$ using a 1D causal transformer backbone with RoPE temporal embeddings. Individual tokens are obtained by passing pos and rot through separate positional embedders, concatenating fov and applying a linear projection. W is cropped to its inner-most 4^3 voxels and embedded alongside A via a joint MLP prior to AdaLN injection. Given that the camera only rotates along its pitch and yaw axis, we re-parametrise the model’s output layer to predict $\bar{c} = \langle \text{pos}, \Delta \text{pitch}, \Delta \text{yaw}, \Delta \text{fov} \rangle$, with residuals $\Delta \text{pitch} = \text{pitch}_t - \text{pitch}_{t-1}$, $\Delta \text{yaw} = \text{yaw}_t - \text{yaw}_{t-1}$ and $\Delta \text{fov} = \text{fov}_t - \text{fov}_{t-1}$.³ The camera model is trained via MSE losses applied to each component of \bar{c} .

5.2. World-to-Pixel Generation

In order to condition the pixel-space generation on 3D information we need to form world-to-pixel correspondence.

World projection. We project w to screen-space via the projection operator

$$\mathcal{R}(c, w) = (\tilde{w}_{2D}, d), \quad (5)$$

where $\tilde{w}_{2D} \in \mathbb{R}^{h \times w \times l \times m}$ is a per-pixel depth-ordered list of l voxel features with m channels, indexed according to their position in screen space $\langle h_i, w_j \rangle$. $d \in \mathbb{R}^{h \times w \times l}$ is the linear depth of each voxel feature measured in camera space. We provide a visualisation of how \mathcal{R} constructs \tilde{w}_{2D} and d in Figure 4. \mathcal{R} employs the same h, w screen dimensions as the pixel latents, ensuring pixel-level alignment with \bar{o} . Finally, we combine \tilde{w}_{2D} and d into $w_{2D} \in \mathbb{R}^{h \times w \times z}$ via channel-wise concatenation, where $z = l \times (m + 1)$.

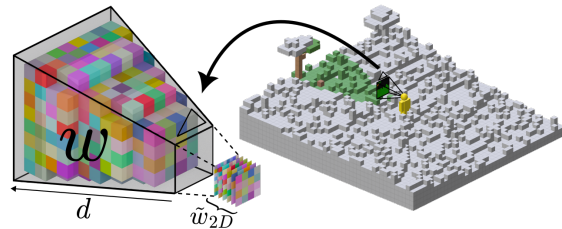


Figure 4. World frame w features are projected to screen-space to obtain the depth-ordered stack of features \tilde{w}_{2D} and linear depth information d .

Pixel frame prediction. Pixel frames are generated by

³ c_t is recovered from $\langle \bar{c}_t, c_{t-1} \rangle$ via an algebraic manipulation at inference time.

sampling

$$\bar{o}_t \sim \mathcal{P}_\theta(\bar{o}_t | W_{2D_{t-K}}^t, A_{t-K}^t, \bar{O}_{t-K}^{t-1}), \quad (6)$$

where $W_{2D_{t-K}}^t$ is obtained from the projection $\mathcal{R}(C_{t-K}^t, W_{t-K}^t)$. Here, \mathcal{P}_θ acts as a learned deferred shader (Thies et al., 2019) which additionally predicts information not provided by 3D latents (e.g. texture, lighting, particle effects, screen-space overlays, ...). This choice allows \mathcal{P}_θ to learn arbitrary rendering functions, whilst encouraging spatial consistency through its dependency on w_{2D} . \mathcal{P}_θ is parametrised as a rectified flow model with a causal DiT backbone employing interleaved spatial and temporal modules (Decart et al., 2024). Actions are embedded using a MLP and injected via AdaLN. w_{2D} is projected to latent space via a channel-wise 1D-convolution and is incorporated to \bar{o} via channel-wise concatenation. Crucially, we assign more latent channels to w_{2D} than to \bar{o} , in order to bias the model to use the 3D latent frame as its primary source of information.

5.3. Mitigating Exposure Bias

During training, the denoisers condition on latents encoded from the training data. However, they condition on autoregressive predictions at inference time, leading to exposure bias (Ning et al., 2024). We train each diffuser with diffusion forcing (Chen et al., 2024) to make them robust to the exposure bias induced by their own predictions. In addition, at inference \mathcal{W}_θ depends on latents predicted by \mathcal{P}_θ , and vice-versa. To alleviate the resulting distributional shift, we apply a flat 10% random noise augmentation to \bar{O} when training \mathcal{W}_θ , and to \bar{W} when training \mathcal{P}_θ . This lets us train each component of PERSIST separately and combine them at inference time without any fine-tuning.

6. Experiments

We conduct our experiments within Luantu (Luantu contributors, 2024), an open-source voxel-based game engine inspired by Minecraft.⁴ Voxel environments discretise 3D space into individual voxels, each voxel taking on any of thousands of possible configurations (e.g. water, stone, air, etc.). These environments constitute a valuable research platform (Malagón et al., 2025; Fan et al., 2022; Guss et al., 2019; Baker et al., 2022), as they instantiate interpretable, complex, diverse, and persistent 3D worlds with rich player–environment interactions. Unlike prior work that learns world models from data collected within a single game map (Alonso et al., 2024; Kanervisto et al., 2025), we learn a broad distribution of procedurally generated worlds. Training world models within procedural environments sub-

⁴We prefer Luantu over Minecraft due to its open-source design and expressive Lua API, which facilitates data collection and experimentation.

stantially increases the difficulty of achieving spatial and temporal consistency, as the model cannot overfit to a fixed environment layout.

Dataset. We use the Craftium platform (Malagón et al., 2025) to collect game data to train and evaluate our models. We collect ~ 40 M environment interactions consisting of player actions, camera states, pixel and 3D observations. Actions are represented as multi-hot vectors encoding individual key presses and discretised mouse movements. 3D observations are represented as a 48^3 voxel grid centred on the agent. In Luantu, individual voxels contain semantic information about a specific spatial location, encoded as integer labels. In total, we collect ~ 100 K trajectories, amounting to 460 hours of gameplay recorded at 24Hz. To interact with the game, we employ a similar strategy as (Yu et al., 2025) and design a simple policy that randomly samples from a set of pre-defined action sequences.

Training and Inference. All models are trained using the AdamW (Loshchilov & Hutter, 2019) optimizer with a learning rate of $1e-4$. We first train the VAEs and pre-encode the 3D and pixel latents to accelerate the training of the dynamic models. The pixel and 3D VAEs take 4 and 12 days to train using 8 A100 GPUs. We train two versions of the 3D denoiser, “3D-S” and “3D-XL”, which uses $8\times$ more spatial tokens. 3D-Small takes 3 days to train on 8 H100 GPUs, while 3D-XL and the pixel denoiser each take 10 days. The camera model trains on a single A100 in 16 hours with batch size 256. All other models use batch size 64. Each model is trained separately and assembled in the full pipeline with no further finetuning. At inference, we use 20 denoising steps per-frame and slightly noise past context frames to make the denoisers more resilient to imperfections in their own generations. We provide more implementation details in Appendix A.

6.1. Interactive Generation

In this section, we assess our method’s ability to generate interactive experiences that are both spatially and temporally consistent. We craft action policies specifically designed to make the agent explore its environment while continually revisiting previously rendered locations at different times and from various viewpoints. We deploy these policies in Craftium to collect a dataset of 148 evaluation trajectories from game worlds that were held-out from the training set. Finally, we sample starting conditions $\langle o_0, c_0 \rangle$ and action sequences from the evaluation set to generate trajectories with PERSIST-S (featuring the 3D-S denoiser) and PERSIST-XL (featuring the 3D-XL denoiser).

Baselines. We compare our approach with Oasis (Decart et al., 2024) and WorldMem (Xiao et al., 2025b), two interactive video generation methods employing the same DiT backbone as \mathcal{P}_θ , but only conditioning on observations

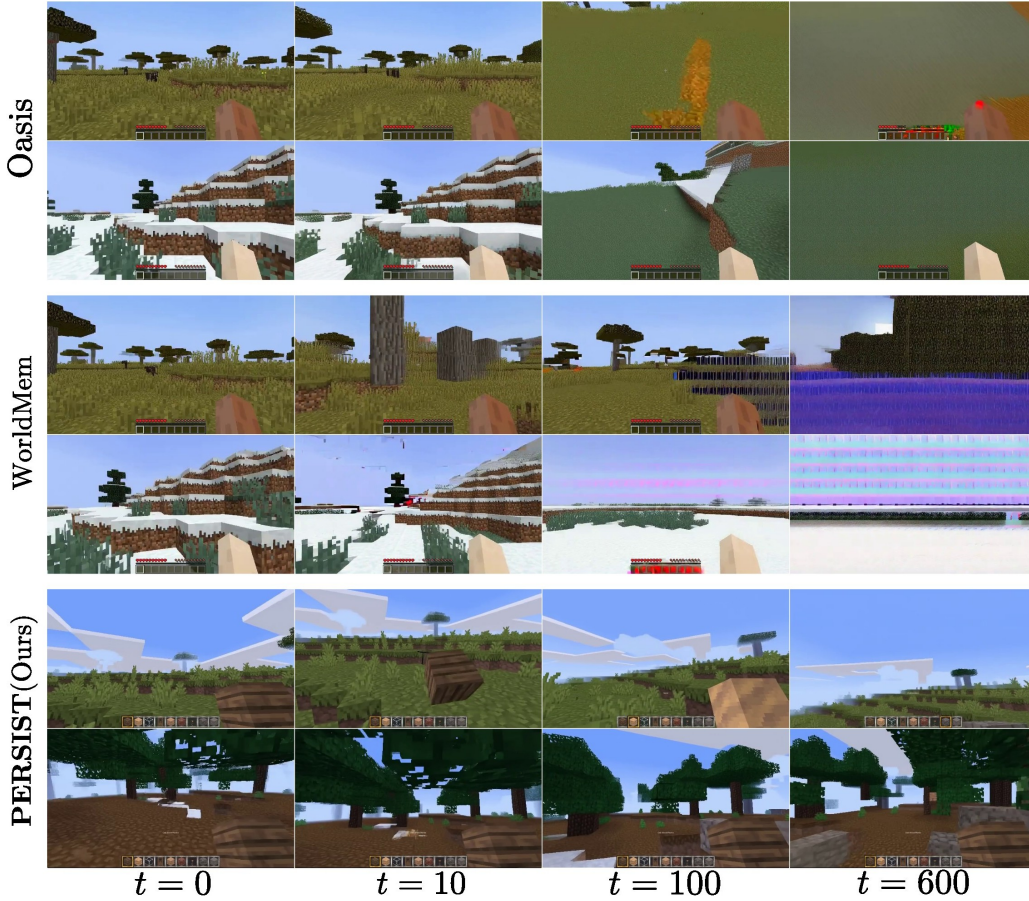


Figure 5. Video frames generated over 600 timestep episodes by PERSIST (Ours), Oasis (Decart et al., 2024) and WorldMem (Xiao et al., 2025a).

sampled from O^{t-1} . Oasis conditions on the most recent O_{t-K}^{t-1} observations, and can therefore also be viewed as an ablation of PERSIST in which the guidance provided by W_{2D} is disabled. WorldMem tracks camera states during generation, and guides generation by retrieving from the full history key-frames closely matching the current camera state. As these methods were trained using Minecraf data, we collect a separate evaluation set in Minedojo (Fan et al., 2022) to not induce domain shift, and we replicate their respective inference configurations. In the case of WorldMem, this includes initialising the memory bank used to sample key-frames with 600 ground truth cameras and pixel observations. This contrasts with PERSIST, which is initialised from a single initial frame $\langle o_0, c_0 \rangle$.

Evaluation. We conduct an user study comprising over 800 rollout evaluations from 28 participants. Users rate each video on “Per-Frame Visual Fidelity”, “3D Spatial Consistency”, and “Temporal Environment Stability and Consistency” before assigning an overall score. We additionally report the Frechet Video Distance (FVD) (Unterthiner et al., 2018) between each method and its corresponding

evaluation set. While the FVD captures distribution-level discrepancies, it has a bias to favour per-frame visual quality over temporal consistency (Ge et al., 2024). In contrast, human ratings directly assess spatial and temporal coherence within individual episodes, making the two complementary. Results are summarised in Table 1, with full methodological details in Appendix B and extended results in Appendix C.

Across all metrics, PERSIST configurations consistently outperform the baselines, highlighting the benefits of explicitly maintaining a persistent 3D environment state. Improvements in FVD and per-frame visual fidelity further indicate that guidance from w_{2D} enhances visual quality. Qualitative rollouts (Figure 5) corroborate these findings, particularly over long horizons.

Spatial resolution of W_θ . While PERSIST-XL achieves a lower FVD than PERSIST-S, we find that the two configurations perform similarly in terms of average user ratings and during head-to-head comparisons (see Appendix C). This suggests that the effectiveness of the 3D representation is robust to reductions in the spatial resolution of W_θ .

Table 1. FVD and mean user ratings (score range: 1-5) for videos generated from different PERSIST configurations and baselines. Bold numbers indicate the best performing methods. We find that every PERSIST configuration significantly outperforms baselines for all measured metrics. PERSIST-XL+ w_0 is discussed in Section 6.2.

Method	FVD↓	Per Frame Visual Fidelity↑	3D Consistency↑	Temporal Consistency↑	Overall Score↑
Oasis	706	2.1 ± 0.1	1.9 ± 0.1	1.8 ± 0.1	1.9 ± 0.1
WorldMem	596	1.7 ± 0.09	1.7 ± 0.09	1.5 ± 0.08	1.5 ± 0.07
PERSIST-S	209	2.8 ± 0.1	2.7 ± 0.1	2.5 ± 0.1	2.6 ± 0.09
PERSIST-XL	181	2.8 ± 0.09	2.5 ± 0.09	2.5 ± 0.09	2.6 ± 0.08
PERSIST-XL+ w_0	116	3.2 ± 0.1	2.8 ± 0.1	2.8 ± 0.1	3.0 ± 0.1

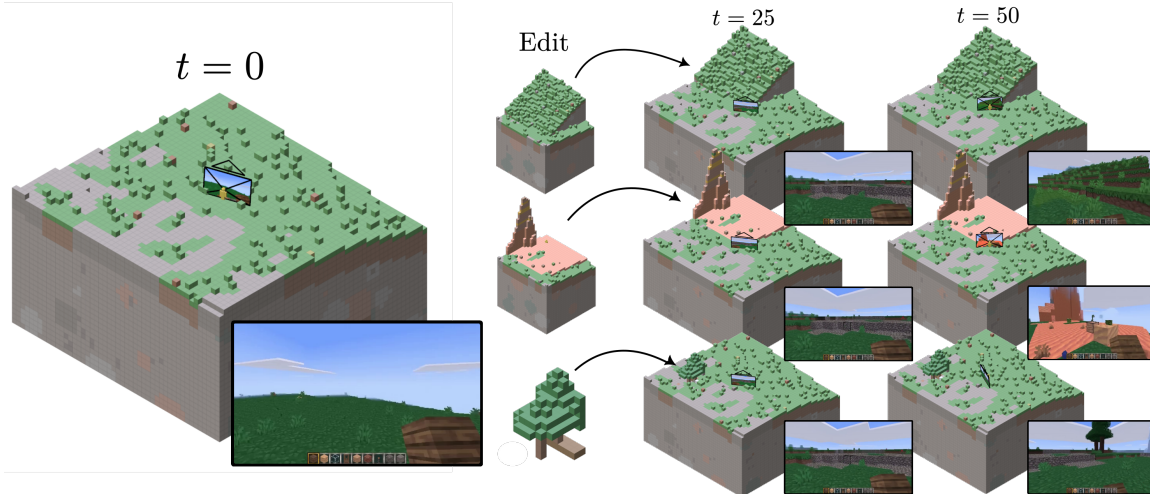


Figure 6. PERSIST’s explicit 3D representation allows us to edit the world-state during an episode, enabling intuitive fine grained control over generations. We demonstrate this above with both global edits to terrain and biome, as well as the placement of smaller assets such as trees.

6.2. New Applications and Emerging Capabilities

In addition to its improvement to the quality and coherence of generated experiences, we find that PERSIST’s 3D representation confers a number of new capabilities.

3D generation. At initialisation, it is essential for w_0 to capture the structure and semantics of the provided conditioning RGB observation. In Figure 13, we show that \mathcal{W}_θ successfully generates plausible starting world frames, while also outpainting unseen regions differently from one episode to the next. This ability lets PERSIST generate environments that are both diverse and coherent, supporting a wide variety of interactive experiences.

Explicit 3D initialisation. By default, PERSIST initialises generation from starting condition $\langle o_0, c_0 \rangle$, with the initial world-frame w_0 being inferred by the world dynamics model \mathcal{W}_θ . However PERSIST also supports w_0 being provided as a starting condition. This explicit 3D conditioning allows a greater degree of control over the generated experience than providing an image, as the full surroundings of the agent can be specified.

To assess how effectively PERSIST can leverage explicit 3D conditioning, we evaluate a variant denoted PERSIST-XL+ w_0 , where a ground-truth world-frame w_0 is provided at initialisation. PERSIST-XL+ w_0 improves over PERSIST-XL in terms of FVD and human ratings (Table 1), demonstrating that the model successfully incorporates the additional information contained within w_0 .

World edits mid-generation. Valevski et al. (2024a) and Kanervisto et al. (2025) proposed to perform manual edits to generated pixel frames before re-injecting them as context, as an alternative way of controlling the generated experience. Similarly, as we can extract w_t at any point during generation, we obtain the capability of making precise 3D-edits to the world mid-episode. To do so, we pause generation after timestep t and manually edit w_t to obtain \tilde{w}_t . We then restart generation using $\{\tilde{w}_t, c_t, o_t, a_t\}$ as the starting condition. We show several edit examples in Figure 6.

Persistent world dynamics. PERSIST learns to model environmental processes that evolve on their own. In Figure 7

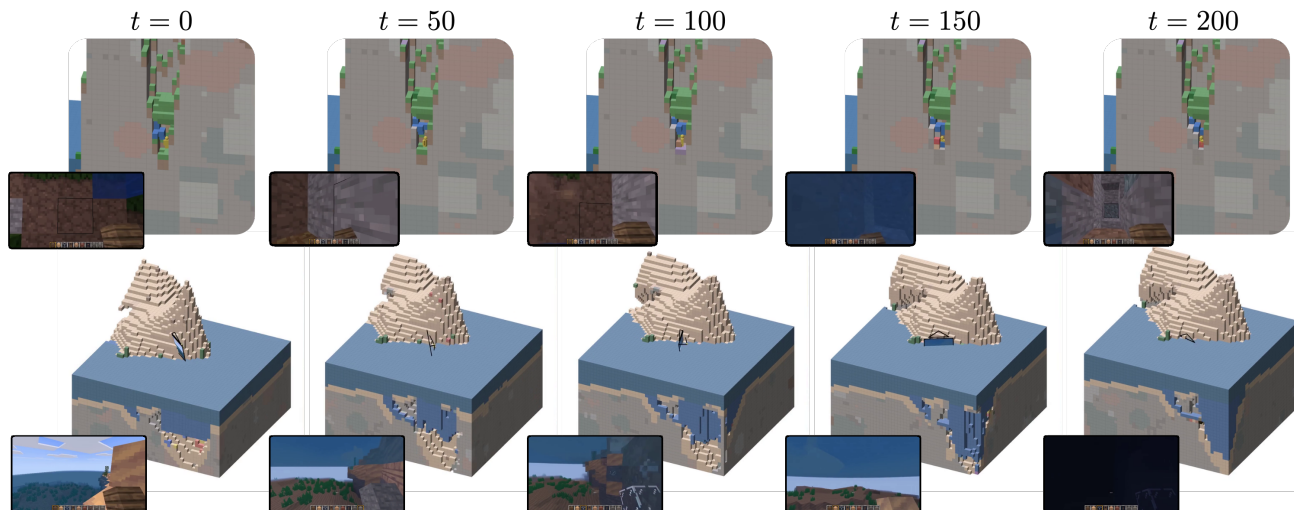


Figure 7. PERSIST maintains a dynamic 3D state that evolves even when unobserved (bottom: a cave filling with water), allowing off-screen events to produce on-screen effects (top: water flowing onto the player at $t = 150$).

we provide examples of environment changes occurring outside of the agent’s view, sometimes giving rise to unexpected interactions, e.g. water flowing onto the agent from above.

7. Conclusion

In this work, we introduced PERSIST, a world modelling framework that tracks the evolution of a persistent latent 3D state. Our results demonstrate that actively generating guidance frames from this 3D state substantially improves spatial memory, temporal coherence, and overall generation quality compared to conditioning on pixel-based histories. We show that tracking this 3D world state allows the model to capture environment dynamics occurring beyond the agent’s view. Additionally, it lets users pre-specify, visualise, and modify the structure of generated environments, creating new ways of controlling generated experiences.

Despite these advances, PERSIST currently relies on ground-truth 3D supervision during training, and faces challenges common to AR generation, such as error accumulation and memory constraints. We report examples of generation glitches caused by error accumulation over the course of a 2000 steps episode in Figure 14. We believe these limitations outline a clear roadmap for future research involving persistent 3D world states: in-the-wild training via synthetic 3D annotations obtained from 2D-to-3D foundation models (Wang et al., 2025; Team et al., 2025), end-to-end post-training on generated rollouts to mitigate autoregressive drift (Huang et al., 2025c), and access to unconstrained spatial memory via a 3D memory bank. We provide a detailed discussion of these directions in Appendix D.

Impact Statement

This work advances the field of Machine Learning by improving the spatial and temporal consistency of generative world models. While our research is primarily conducted within the simulated environment of Luanti, the underlying methodologies have potential applications in video games, digital twin simulation, and embodied AI navigation, where reliable 3D scene representation is critical. We do not foresee any immediate negative societal consequences that require specific highlighting at this stage, as our model operates within a synthetic domain.

References

- Albergo, M. S. and Vanden-Eijnden, E. Building normalizing flows with stochastic interpolants. In *The Eleventh International Conference on Learning Representations, ICLR 2023, Kigali, Rwanda, May 1-5, 2023*. OpenReview.net, 2023. URL <https://openreview.net/pdf?id=li7qeBbCR1t>.
- Alonso, E., Jelley, A., Micheli, V., Kanervisto, A., Storkey, A. J., Pearce, T., and Fleuret, F. Diffusion for world modeling: Visual details matter in atari. In Globersons, A., Mackey, L., Belgrave, D., Fan, A., Paquet, U., Tomczak, J. M., and Zhang, C. (eds.), *Advances in Neural Information Processing Systems 38: Annual Conference on Neural Information Processing Systems 2024, NeurIPS 2024, Vancouver, BC, Canada, December 10 - 15, 2024*, 2024. URL http://papers.nips.cc/paper_files/paper/2024/hash/6bdde0373d53d4a501249547084bed43-Abstract-Conference.html.

- Baker, B., Akkaya, I., Zhokhov, P., Huizinga, J., Tang, J., Ecoffet, A., Houghton, B., Sampedro, R., and Clune, J. Video pretraining (VPT): learning to act by watching unlabeled online videos. In Koyejo, S., Mohamed, S., Agarwal, A., Belgrave, D., Cho, K., and Oh, A. (eds.), *Advances in Neural Information Processing Systems 35: Annual Conference on Neural Information Processing Systems 2022, NeurIPS 2022, New Orleans, LA, USA, November 28 - December 9, 2022*, 2022. URL http://papers.nips.cc/paper_files/paper/2022/hash/9c7008aff45b5d8f0973b23e1a22ada0-Abstract-Conference.html.
- Ball, P. J., Bauer, J., Belletti, F., Brownfield, B., Ephrat, A., Fruchter, S., Gupta, A., Holsheimer, K., Holynski, A., Hron, J., Kaplanis, C., Limont, M., McGill, M., Oliveira, Y., Parker-Holder, J., Perbet, F., Scully, G., Shar, J., Spencer, S., Tov, O., Villegas, R., Wang, E., Yung, J., Baetu, C., Berbel, J., Bridson, D., Bruce, J., Buttimore, G., Chakera, S., Chandra, B., Collins, P., Cullum, A., Damoc, B., Dasagi, V., Gazeau, M., Gbadamosi, C., Han, W., Hirst, E., Kachra, A., Kerley, L., Kjems, K., Knoepfel, E., Koriakin, V., Lo, J., Lu, C., Mehring, Z., Moufarek, A., Nandwani, H., Oliveira, V., Pardo, F., Park, J., Pierson, A., Poole, B., Ran, H., Salimans, T., Sanchez, M., Saprykin, I., Shen, A., Sidhwani, S., Smith, D., Stanton, J., Tomlinson, H., Vijaykumar, D., Wang, L., Wingfield, P., Wong, N., Xu, K., Yew, C., Young, N., Zubov, V., Eck, D., Erhan, D., Kavukcuoglu, K., Hassabis, D., Gharamani, Z., Hadsell, R., van den Oord, A., Mosseri, I., Bolton, A., Singh, S., and Rocktäschel, T. Genie 3: A new frontier for world models. 2025.
- Bavoil, L. and Myers, K. Order independent transparency with dual depth peeling. *NVIDIA OpenGL SDK*, 1(12): 2–4, 2008.
- Carreira, J. and Zisserman, A. Quo vadis, action recognition? A new model and the kinetics dataset. In *2017 IEEE Conference on Computer Vision and Pattern Recognition, CVPR 2017, Honolulu, HI, USA, July 21-26, 2017*, pp. 4724–4733. IEEE Computer Society, 2017. doi: 10.1109/CVPR.2017.502. URL <https://doi.org/10.1109/CVPR.2017.502>.
- Chang, A., Dai, A., Funkhouser, T., Halber, M., Niessner, M., Savva, M., Song, S., Zeng, A., and Zhang, Y. Matterport3d: Learning from rgb-d data in indoor environments. *International Conference on 3D Vision (3DV)*, 2017.
- Che, H., He, X., Liu, Q., Jin, C., and Chen, H. Gamegenx: Interactive open-world game video generation. In *The Thirteenth International Conference on Learning Representations*, 2024.
- Chen, B., Monso, D. M., Du, Y., Simchowitz, M., Tedrake, R., and Sitzmann, V. Diffusion forcing: Next-token prediction meets full-sequence diffusion. In Globersons, A., Mackey, L., Belgrave, D., Fan, A., Paquet, U., Tomczak, J. M., and Zhang, C. (eds.), *Advances in Neural Information Processing Systems 38: Annual Conference on Neural Information Processing Systems 2024, NeurIPS 2024, Vancouver, BC, Canada, December 10 - 15, 2024*, 2024. URL http://papers.nips.cc/paper_files/paper/2024/hash/2aeelc4159e48407d68fe16ae8e6e49e-Abstract-Conference.html.
- Chen, Z., Funkhouser, T. A., Hedman, P., and Tagliasacchi, A. Mobilenerf: Exploiting the polygon rasterization pipeline for efficient neural field rendering on mobile architectures. In *IEEE/CVF Conference on Computer Vision and Pattern Recognition, CVPR 2023, Vancouver, BC, Canada, June 17-24, 2023*, pp. 16569–16578. IEEE, 2023. doi: 10.1109/CVPR52729.2023.01590. URL <https://doi.org/10.1109/CVPR52729.2023.01590>.
- Decart, Quevedo, J., McIntyre, Q., Campbell, S., Chen, X., and Wachen, R. Oasis: A universe in a transformer. 2024. URL <https://oasis-model.github.io/>.
- Deering, M., Winner, S., Schediwy, B., Duffy, C., and Hunt, N. The triangle processor and normal vector shader: a vlsi system for high performance graphics. *ACM Siggraph Computer Graphics*, 22(4):21–30, 1988.
- Dosovitskiy, A., Beyer, L., Kolesnikov, A., Weissenborn, D., Zhai, X., Unterthiner, T., Dehghani, M., Minderer, M., Heigold, G., Gelly, S., Uszkoreit, J., and Houlsby, N. An image is worth 16x16 words: Transformers for image recognition at scale. In *9th International Conference on Learning Representations, ICLR 2021, Virtual Event, Austria, May 3-7, 2021*. OpenReview.net, 2021. URL <https://openreview.net/forum?id=YicbFdNTTy>.
- Fan, L., Wang, G., Jiang, Y., Mandlekar, A., Yang, Y., Zhu, H., Tang, A., Huang, D., Zhu, Y., and Anandkumar, A. Minedojo: Building open-ended embodied agents with internet-scale knowledge. In Koyejo, S., Mohamed, S., Agarwal, A., Belgrave, D., Cho, K., and Oh, A. (eds.), *Advances in Neural Information Processing Systems 35: Annual Conference on Neural Information Processing Systems 2022, NeurIPS 2022, New Orleans, LA, USA, November 28 - December 9, 2022*, 2022. URL http://papers.nips.cc/paper_files/paper/2022/hash/74a67268c5cc5910f64938cac4526a90-Abstract-Datasets_and_Benchmarks.html.

- Garcin, S., Doran, J., Guo, S., Lucas, C. G., and Albrecht, S. V. DRED: zero-shot transfer in reinforcement learning via data-regularised environment design. In *Forty-first International Conference on Machine Learning, ICML 2024, Vienna, Austria, July 21-27, 2024*. OpenReview.net, 2024. URL <https://openreview.net/forum?id=uku9r6RR0l>.
- Ge, S., Mahapatra, A., Parmar, G., Zhu, J., and Huang, J. On the content bias in fréchet video distance. In *IEEE/CVF Conference on Computer Vision and Pattern Recognition, CVPR 2024, Seattle, WA, USA, June 16-22, 2024*, pp. 7277–7288. IEEE, 2024. doi: 10.1109/CVPR52733.2024.00695. URL <https://doi.org/10.1109/CVPR52733.2024.00695>.
- Guss, W. H., Houghton, B., Topin, N., Wang, P., Codel, C., Veloso, M., and Salakhutdinov, R. Minerl: A large-scale dataset of minecraft demonstrations. In Kraus, S. (ed.), *Proceedings of the Twenty-Eighth International Joint Conference on Artificial Intelligence, IJCAI 2019, Macao, China, August 10-16, 2019*, pp. 2442–2448. ijcai.org, 2019. doi: 10.24963/ijcai.2019/339. URL <https://doi.org/10.24963/ijcai.2019/339>.
- Ha, D. and Schmidhuber, J. World models. 2018. doi: 10.5281/ZENODO.1207631. URL <https://zenodo.org/record/1207631>.
- Hafner, D., Yan, W., and Lillicrap, T. Training agents inside of scalable world models. *arXiv preprint arXiv: 2509.24527*, 2025.
- He, X., Peng, C., Liu, Z., Wang, B., Zhang, Y., Cui, Q., Kang, F., Jiang, B., An, M., Ren, Y., et al. Matrix-game 2.0: An open-source, real-time, and streaming interactive world model. *ArXiv preprint*, abs/2508.13009, 2025. URL <https://arxiv.org/abs/2508.13009>.
- Huang, J., Hu, X., Han, B., Shi, S., Tian, Z., He, T., and Jiang, L. Memory forcing: Spatio-temporal memory for consistent scene generation on minecraft. *arXiv preprint arXiv: 2510.03198*, 2025a.
- Huang, T., Zheng, W., Wang, T., Liu, Y., Wang, Z., Wu, J., Jiang, J., Li, H., Lau, R., Zuo, W., et al. Voyager: Long-range and world-consistent video diffusion for explorable 3d scene generation. *ACM Transactions on Graphics (TOG)*, 44(6):1–15, 2025b.
- Huang, X., Li, Z., He, G., Zhou, M., and Shechtman, E. Self forcing: Bridging the train-test gap in autoregressive video diffusion. *ArXiv preprint*, abs/2506.08009, 2025c. URL <https://arxiv.org/abs/2506.08009>.
- Kanervisto, A., Bignell, D., Wen, L. Y., Grayson, M., Georgescu, R., Valcarcel Macua, S., Tan, S. Z., Rashid, T., Pearce, T., Cao, Y., et al. World and human action models towards gameplay ideation. *Nature*, 638(8051): 656–663, 2025.
- Labs, W. Marble: A multimodal world model. <https://www.worldlabs.ai/blog/marble-world-model>, 2025. Blog Post. Accessed: 2026-01-29.
- Li, Z., Müller, T., Evans, A., Taylor, R. H., Unberath, M., Liu, M., and Lin, C. Neuralangelo: High-fidelity neural surface reconstruction. In *IEEE/CVF Conference on Computer Vision and Pattern Recognition, CVPR 2023, Vancouver, BC, Canada, June 17-24, 2023*, pp. 8456–8465. IEEE, 2023. doi: 10.1109/CVPR52729.2023.00817. URL <https://doi.org/10.1109/CVPR52729.2023.00817>.
- Lipman, Y., Chen, R. T. Q., Ben-Hamu, H., Nickel, M., and Le, M. Flow matching for generative modeling. In *The Eleventh International Conference on Learning Representations, ICLR 2023, Kigali, Rwanda, May 1-5, 2023*. OpenReview.net, 2023. URL <https://openreview.net/pdf?id=PqvMRDCJT9t>.
- Loshchilov, I. and Hutter, F. Decoupled weight decay regularization. In *7th International Conference on Learning Representations, ICLR 2019, New Orleans, LA, USA, May 6-9, 2019*. OpenReview.net, 2019. URL <https://openreview.net/forum?id=Bkg6RiCqY7>.
- Luanti contributors. Luanti: An open source voxel game-creation platform. <https://github.com/luanti-org/luanti>, 2024. Formerly Minetest.
- Malagón, M., Ceberio, J., and Lozano, J. A. Craftium: Bridging flexibility and efficiency for rich 3d single- and multi-agent environments. In *International Conference on Machine Learning (ICML)*, 2025.
- Micheli, V., Alonso, E., and Fleuret, F. Transformers are sample-efficient world models. In *The Eleventh International Conference on Learning Representations, ICLR 2023, Kigali, Rwanda, May 1-5, 2023*. OpenReview.net, 2023. URL <https://openreview.net/pdf?id=vhFulAcb0xb>.
- Mildenhall, B., Srinivasan, P. P., Tancik, M., Barron, J. T., Ramamoorthi, R., and Ng, R. Nerf: Representing scenes as neural radiance fields for view synthesis. *Communications of the ACM*, 65(1):99–106, 2021.
- Müller, T., Evans, A., Schied, C., and Keller, A. Instant neural graphics primitives with a multiresolution hash encoding. *ACM transactions on graphics (TOG)*, 41(4): 1–15, 2022.

- Nagy, Z. and Klein, R. Depth-peeling for texture-based volume rendering. In *11th Pacific Conference on Computer Graphics and Applications, 2003. Proceedings.*, pp. 429–433. IEEE, 2003.
- Ning, M., Li, M., Su, J., Salah, A. A., and Ertugrul, I. Ö. Elucidating the exposure bias in diffusion models. In *The Twelfth International Conference on Learning Representations, ICLR 2024, Vienna, Austria, May 7-11, 2024*. OpenReview.net, 2024. URL <https://openreview.net/forum?id=xEJMojlSpX>.
- Peebles, W. and Xie, S. Scalable diffusion models with transformers. In *IEEE/CVF International Conference on Computer Vision, ICCV 2023, Paris, France, October 1-6, 2023*, pp. 4172–4182. IEEE, 2023. doi: 10.1109/ICCV51070.2023.00387. URL <https://doi.org/10.1109/ICCV51070.2023.00387>.
- Po, R., Nitzan, Y., Zhang, R., Chen, B., Dao, T., Shechtman, E., Wetzstein, G., and Huang, X. Long-context state-space video world models. In *Proceedings of the IEEE/CVF International Conference on Computer Vision*, pp. 8733–8744, 2025.
- Sitzmann, V., Rezkikov, S., Freeman, B., Tenenbaum, J., and Durand, F. Light field networks: Neural scene representations with single-evaluation rendering. In Ranzato, M., Beygelzimer, A., Dauphin, Y. N., Liang, P., and Vaughan, J. W. (eds.), *Advances in Neural Information Processing Systems 34: Annual Conference on Neural Information Processing Systems 2021, NeurIPS 2021, December 6-14, 2021, virtual*, pp. 19313–19325, 2021. URL <https://proceedings.neurips.cc/paper/2021/hash/allce019e96a4c60832eadd755a17a58-Abstract.html>.
- Song, K., Chen, B., Simchowitz, M., Du, Y., Tedrake, R., and Sitzmann, V. History-guided video diffusion. *ArXiv preprint*, abs/2502.06764, 2025. URL <https://arxiv.org/abs/2502.06764>.
- Su, J., Ahmed, M., Lu, Y., Pan, S., Bo, W., and Liu, Y. Roformer: Enhanced transformer with rotary position embedding. *Neurocomputing*, 568:127063, 2024.
- Team, S. D., Chen, X., Chu, F.-J., Gleize, P., Liang, K. J., Sax, A., Tang, H., Wang, W., Guo, M., Hardin, T., Li, X., Lin, A., Liu, J., Ma, Z., Sagar, A., Song, B., Wang, X., Yang, J., Zhang, B., Dollár, P., Gkioxari, G., Feiszli, M., and Malik, J. Sam 3d: 3dfy anything in images. *ArXiv preprint*, abs/2511.16624, 2025. URL <https://arxiv.org/abs/2511.16624>.
- Thies, J., Zollhöfer, M., and Nießner, M. Deferred neural rendering: Image synthesis using neural textures. *ACM Transactions on Graphics (TOG)*, 38(4):1–12, 2019.
- Unterthiner, T., Van Steenkiste, S., Kurach, K., Marinier, R., Michalski, M., and Gelly, S. Towards accurate generative models of video: A new metric & challenges. *ArXiv preprint*, abs/1812.01717, 2018. URL <https://arxiv.org/abs/1812.01717>.
- Valevski, D., Leviathan, Y., Arar, M., and Fruchter, S. Diffusion models are real-time game engines, 2024a. URL <https://arxiv.org/abs/2408.14837>.
- Valevski, D., Leviathan, Y., Arar, M., and Fruchter, S. Diffusion models are real-time game engines. In *The Thirteenth International Conference on Learning Representations, 2024b*.
- Walker, T., Mariotti, O., Vaxman, A., and Bilen, H. Explicit neural surfaces: Learning continuous geometry with deformation fields. *ArXiv preprint*, abs/2306.02956, 2023. URL <https://arxiv.org/abs/2306.02956>.
- Wang, J., Chen, M., Karaev, N., Vedaldi, A., Rupprecht, C., and Novotny, D. Vggt: Visual geometry grounded transformer. In *Proceedings of the IEEE/CVF Conference on Computer Vision and Pattern Recognition, 2025*.
- Worchel, M., Diaz, R., Hu, W., Schreer, O., Feldmann, I., and Eisert, P. Multi-view mesh reconstruction with neural deferred shading. In *Proceedings of the IEEE/CVF Conference on Computer Vision and Pattern Recognition*, pp. 6187–6197, 2022.
- Xiang, J., Lv, Z., Xu, S., Deng, Y., Wang, R., Zhang, B., Chen, D., Tong, X., and Yang, J. Structured 3d latents for scalable and versatile 3d generation. *Cvpr*, 2025.
- Xiao, Z., Lan, Y., Zhou, Y., Ouyang, W., Yang, S., Zeng, Y., and Pan, X. Worldmem: Long-term consistent world simulation with memory. *ArXiv preprint*, abs/2504.12369, 2025a. URL <https://arxiv.org/abs/2504.12369>.
- Xiao, Z., Lan, Y., Zhou, Y., Ouyang, W., Yang, S., Zeng, Y., and Pan, X. Worldmem: Long-term consistent world simulation with memory, 2025b. URL <https://arxiv.org/abs/2504.12369>.
- Yeshwanth, C., Liu, Y., Nießner, M., and Dai, A. ScanNet++: A high-fidelity dataset of 3d indoor scenes. In *IEEE/CVF International Conference on Computer Vision, ICCV 2023, Paris, France, October 1-6, 2023*, pp. 12–22. IEEE, 2023. doi: 10.1109/ICCV51070.2023.00008. URL <https://doi.org/10.1109/ICCV51070.2023.00008>.
- Yu, J., Qin, Y., Wang, X., Wan, P., Zhang, D., and Liu, X. Gamefactory: Creating new games with generative interactive videos. *ArXiv preprint*, abs/2501.08325, 2025. URL <https://arxiv.org/abs/2501.08325>.

Zhang, Y., Peng, C., Wang, B., Wang, P., Zhu, Q., Kang, F., Jiang, B., Gao, Z., Li, E., Liu, Y., et al. Matrix-game: Interactive world foundation model. *ArXiv preprint*, abs/2506.18701, 2025. URL <https://arxiv.org/abs/2506.18701>.

Zhou, S., Du, Y., Yang, Y., Han, L., Chen, P., Yeung, D.-Y., and Gan, C. Learning 3d persistent embodied world models. *ArXiv preprint*, abs/2505.05495, 2025. URL <https://arxiv.org/abs/2505.05495>.

Zhou, T., Tucker, R., Flynn, J., Fyffe, G., and Snavely, N. Stereo magnification: Learning view synthesis using multiplane images. *ArXiv preprint*, abs/1805.09817, 2018. URL <https://arxiv.org/abs/1805.09817>.

Zhou, Y., Barnes, C., Lu, J., Yang, J., and Li, H. On the continuity of rotation representations in neural networks. In *IEEE Conference on Computer Vision and Pattern Recognition, CVPR 2019, Long Beach, CA, USA, June 16-20, 2019*, pp. 5745–5753. Computer Vision Foundation / IEEE, 2019. doi: 10.1109/CVPR.2019.00589. URL http://openaccess.thecvf.com/content_CVPR_2019/html/Zhou_On_the_Continuity_of_Rotation_Representations_in_Neural_Networks_CVPR_2019_paper.html.

A. Additional Implementation Details

A.1. Additional Model Details

2D VAE. We employ a vision transformer architecture (Dosovitskiy et al., 2021), using the open-source implementation of (Decart et al., 2024). We train the VAE via an MSE reconstruction objective, alongside a KL divergence penalty coefficient of $1e - 6$.

3D VAE. We employ a 3D-ResNet architecture based on the implementation provided by (Xiang et al., 2025). We train the VAE via a cross-entropy loss to predict voxel class labels, alongside a KL divergence penalty coefficient of $1e - 6$.

Differentiable Rasterizer. For our projecting function \mathcal{R} , we leverage GPU-native triangle rasterization, by assigning voxel features to faces of a static voxel-grid mesh. Then, depth-peeling (Bavoil & Myers, 2008; Nagy & Klein, 2003) is applied during rasterization to produce a per-pixel, depth-ordered stack of 3D features $W_{2D}^t \in \mathbb{R}^{H \times W \times L \times C}$, where L is the maximum number of layers. Since the mesh topology is fixed for a given resolution, we construct it once at initialisation, updating vertex attributes in-place to avoid redundant mesh construction.

A.2. PERSIST and PERSIST+ w_0 Inference Logic

Algorithm 1 PERSIST inference logic.

Input: Models $\mathcal{W}_\theta, \mathcal{C}_\theta, \mathcal{P}_\theta$, 2D-VAE, 3D-VAE,

Model context window sizes K_W, K_C, K_P ,

Renderer \mathcal{R} ,

Initial conditions $o_{\text{init}}, c_{\text{init}}$,

Episode Length T ,

Agent.

- 1: $a_{\text{init}} \leftarrow \text{NO-OP}$
 - 2: $\bar{o}_0 \leftarrow \text{2D-VAE.encode}(o_{\text{init}})$
 - 3: $\bar{w}_0 \leftarrow \mathcal{W}_\theta(a_{\text{init}}, c_{\text{init}}, \bar{o}_0)$
 - 4: $w_0 \leftarrow \text{3D-VAE.decode}(\bar{w}_0)$
 - 5: $w_{2D_0} \leftarrow \mathcal{R}(w_0, c_{\text{init}})$
 - 6: $\bar{o}_0 \leftarrow \mathcal{P}(w_{2D_0}, a_{\text{init}})$
 - 7: $o_0 \leftarrow \text{2D-VAE.decode}(\bar{o}_0)$
 - 8: Initialise rollout buffers $\{A, C, O, \bar{O}, W, \bar{W}, W_{2D}\}$ with
 $a_{\text{init}}, c_{\text{init}}, o_0, \bar{o}_0, w_0, \bar{w}_0, w_{2D_0}$
 - 9: **for** t in $1, \dots, T$ **do**
 - 10: Append to A : $a_t \leftarrow \text{Agent}(o_{t-1})$
 - 11: Append to \bar{W} : $\bar{w}_t \leftarrow \mathcal{W}_\theta(\bar{W}_{t-K_W}^{t-1}, A_{t-K_W}^t, C_{t-K_W-1}^{t-1}, \bar{O}_{t-K_W-1}^{t-1})$
 - 12: Append to W : $w_t \leftarrow \text{3D-VAE.decode}(\bar{w}_t)$
 - 13: Append to C : $c_t \leftarrow \mathcal{C}_\theta(C_{t-1-K_C}^{t-1}, W_{t-K_C}^t, A_{t-K_C}^t)$
 - 14: Append to W_{2D} : $w_{2D_t} \leftarrow \mathcal{R}(w_t, c_t)$
 - 15: Append to \bar{O} : $\bar{o}_t \leftarrow \mathcal{P}_\theta(W_{2D_{t-K_P}}^t, A_{t-K_P}^t, \bar{O}_{t-K_P}^{t-1})$
 - 16: Append to O : $o_t \leftarrow \text{2D-VAE.decode}(\bar{o}_t)$
-

Pipeline is always initialised using a NO-OP action.

Regenerating the starting observation from w_0 guarantees alignment between w_0 and o_0 .

Algorithm 2 PERSIST+ w_0 inference logic. **Changes to Algorithm 1 in blue.**

Input: Models $\mathcal{W}_\theta, \mathcal{C}_\theta, \mathcal{P}_\theta$, 2D-VAE, 3D-VAE,
 Model context window sizes $K_{\mathcal{W}}, K_{\mathcal{C}}, K_{\mathcal{P}}$,
 Renderer \mathcal{R} ,
 Initial conditions $o_{\text{init}}, c_{\text{init}}, w_{\text{init}}$
 Episode Length T ,
 Agent.

- 1: $a_{\text{init}} \leftarrow \text{NO-OP}$
 - 2: $\bar{o}_0 \leftarrow \text{2D-VAE.encode}(o_{\text{init}})$
 - 3: $\bar{w}_0 \leftarrow \text{3D-VAE.encode}(w_{\text{init}})$
 - 4: $w_{2D_0} \leftarrow \mathcal{R}(w_{\text{init}}, c_{\text{init}})$
 - 5: $\bar{o}_0 \leftarrow \text{2D-VAE.encode}(o_{\text{init}})$
 - 6: Initialise rollout buffers $\{A, C, O, \bar{O}, W, \bar{W}, W_{2D}\}$ with
 $a_{\text{init}}, c_{\text{init}}, o_{\text{init}}, \bar{o}_0, w_{\text{init}}, \bar{w}_0, w_{2D_0}$
 - 7: **for** t in $1, \dots, T$ **do**
 - 8: Append to A : $a_t \leftarrow \text{Agent}(o_{t-1})$
 - 9: Append to \bar{W} : $\bar{w}_t \leftarrow \mathcal{W}_\theta(\bar{W}_{t-K_{\mathcal{W}}}^{t-1}, A_{t-K_{\mathcal{W}}}^t, C_{t-K_{\mathcal{W}}-1}^{t-1}, \bar{O}_{t-K_{\mathcal{W}}-1}^{t-1})$
 - 10: Append to W : $w_t \leftarrow \text{3D-VAE.decode}(\bar{w}_t)$
 - 11: Append to C : $c_t \leftarrow \mathcal{C}_\theta(C_{t-1-K_{\mathcal{C}}}^{t-1}, W_{t-K_{\mathcal{C}}}^t, A_{t-K_{\mathcal{C}}}^t)$
 - 12: Append to W_{2D} : $w_{2D_t} \leftarrow \mathcal{R}(w_t, c_t)$
 - 13: Append to \bar{O} : $\bar{o}_t \leftarrow \mathcal{P}_\theta(W_{2D_{t-K_{\mathcal{P}}}}^t, A_{t-K_{\mathcal{P}}}^t, \bar{O}_{t-K_{\mathcal{P}}}^{t-1})$
 - 14: Append to O : $o_t \leftarrow \text{2D-VAE.decode}(\bar{o}_t)$
-

Pipeline is always initialised using a NO-OP action.

We can use o_{init} directly as o_{init} and w_{init} are expected to be perfectly aligned.

A.3. Model and Inference Hyperparameters

Table 2. 3D-VAE configuration.

Parameter	Value
input shape	[48, 48, 48, 2138]
number of residual blocks	2
middle channels	[32, 128, 512]
\bar{w} shape	[12, 12, 12, 48]
# parameters	138M

Table 3. 2D-VAE configuration.

Parameter	Value
input size	[360, 640, 3]
patch size	10
\bar{o} shape	[36, 64, 16]
encoder dimension	1024
encoder depth	6
encoder number of heads	6
decoder dimension	1024
decoder depth	12
decoder number of heads	16
# parameters	227M

Table 4. Camera model configuration.

Parameter	Value
rotation embedding channels	256
translation embedding channels	256
hidden size	1024
transformer blocks	12
number of heads	12
MLP ratio	4
context window size	8
# parameters	234M

Table 5. World denoiser hyperparameters (3D-S configuration). The XL configuration uses patch size=1 and has the same number of learned parameters.

Parameter	Value
input shape	[12, 12, 12, 48]
patch size	2
hidden size	1024
cross condition hidden size	1024
depth	12
number of heads	16
MLP ratio	4
pixel condition patch size	2
context window size	8
# parameters	686M

Table 6. Pixel denoiser configuration.

Parameter	Value
\bar{o} shape	[36, 64, 16]
\bar{o} embedder output channels	16
patch size	2
hidden size	1024
depth	12
number of heads	16
MLP ratio	4
\tilde{w}_{2D} shape	[36, 64, 192, 32]
w_{2D} embedder patch size	6
w_{2D} embedder stride	4
w_{2D} embedder output channels	752
context window size	16
# parameters	460M

Table 7. Flow matching sampler configurations at inference time.

Parameter	Value
minimum noise σ_{\min}	$1e - 5$
denoising steps	20
denoising step scheduling function	$\tau^k = \frac{\eta^k}{1+(\eta-1)k}$
η	3
noise level applied to context (past) frames τ_{ctx}	0.02 (\mathcal{W}_θ) / 0.1 (\mathcal{P}_θ)

Table 8. Number of spatial and temporal tokens for different models.

Model	# Temporal Tokens	# Spatial Tokens
\mathcal{W}_θ -S	8	216
\mathcal{W}_θ -XL	8	1728
\mathcal{P}_θ	16	576
\mathcal{C}_θ	8	n/a

B. Evaluation Methodology

B.1. Evaluation data

As discussed in the main body, we curated evaluation datasets across four modes to assess agent behaviour: *Free Play*, *Move Forward*, *Move Backward*, and *Orbit*. These modes are designed to produce trajectories that require a high level of temporal and spatial consistency to be correctly simulated by the world model.

- **Free Play:** randomly samples action from a set of pre-defined sequences, facilitating exploration.
- **Move Forward/Backward:** The agent moves forwards or backwards, periodically spinning on itself to observe its surroundings.
- **Orbit:** The agent follows a circular trajectory, while constantly adjusting its heading to look towards the centre of the circle.

We collect evaluation sets in MineDojo and Craftium following these policies. For inference with WorldMem, we prepend 600 ground truth frames to each evaluation sequence to warm-start the memory bank.

B.2. FVD computation

To compute the FVD, we collect a total of 148 rollouts of 192 frames for each method, splitting collection evenly across all four evaluation sets. Videos are spliced into 16-frame clips, for a total of 1776 clips. We then compute the FVD from the latent features obtained by passing rollout and ground truth clips through a pretrained Inflated 3D ConvNet (Carreira & Zisserman, 2017).

B.3. User Study Protocol

The user study was deployed via a custom web interface (see Figure 8). Participants were tasked of scoring videos according to the following metrics and instructions:

- **Visual Fidelity.** Per-frame visual quality of the video. Deduct points for visual artifacts such as blurriness, color shifts, flickering, noise, or texture degradation.
- **3D Spatial Consistency.** Spatial consistency of the scene. Deduct points if objects deform, shift, or change appearance when viewed from different camera angles, or if the relative depth and spatial relationships between objects appear inconsistent as the player moves.
- **Temporal Environment Stability and Consistency.** Consistency of the environment over time. Deduct points if the scene changes unexpectedly, such as objects disappearing, reappearing, or changing structure when revisiting previously seen areas, or if the environment degrades or becomes unnaturally simplified over time.
- **Overall Quality Score.** Your subjective rating of the overall quality of the video, considering all factors above.

Ratings had the range of 1-5. Videos were presented to the user as pairs. Each pair depicted matching behaviour (free play, move forward, move backward, orbit) but different methods (baselines, PERSIST configurations, Minedojo or Craftium ground truth). Each individual user was asked to rate up to 50 videos. User assessments were subsequently aggregated to compute average scores. We consider the first three evaluation trials for each participant to count as calibration, and we discard them from the study.

C. Extended User Study Results

C.1. Score Differences During Head-to-Head Comparisons

Given that users rate two side-by-side videos during each trial, we can analyse how a PERSIST configuration fares in a direct head-to-head comparison against any other baseline, PERSIST configuration, or the ground truth data. We provide score comparison matrices below (one per metric) displaying the average score deltas during head-to-head comparisons.

Trial 1 of 25

Please watch both videos before providing your ratings.

Please rate both videos for each metric before continuing.

If a video doesn't load, try refreshing the page.

If the problem persists, click "The video did not load" under that video — you'll then be able to continue without rating it.

Video A

Video B

Metric	Video A	Video B
<p>Visual Fidelity Per-frame visual quality of the video. Deduct points for visual artifacts such as blurriness, color shifts, flickering, noise, or texture degradation.</p>	<input type="radio"/> 1 <input type="radio"/> 2 <input type="radio"/> 3 <input type="radio"/> 4 <input type="radio"/> 5	<input type="radio"/> 1 <input type="radio"/> 2 <input type="radio"/> 3 <input type="radio"/> 4 <input type="radio"/> 5
<p>3D Spatial Consistency Spatial consistency of the scene. Deduct points if objects deform, shift, or change appearance when viewed from different camera angles, or if the relative depth and spatial relationships between objects appear inconsistent as the player moves.</p>	<input type="radio"/> 1 <input type="radio"/> 2 <input type="radio"/> 3 <input type="radio"/> 4 <input type="radio"/> 5	<input type="radio"/> 1 <input type="radio"/> 2 <input type="radio"/> 3 <input type="radio"/> 4 <input type="radio"/> 5
<p>Temporal Environment Stability and Consistency Consistency of the environment over time. Deduct points if the scene changes unexpectedly, such as objects disappearing, reappearing, or changing structure when revisiting previously seen areas, or if the environment degrades or becomes unnaturally simplified over time.</p>	<input type="radio"/> 1 <input type="radio"/> 2 <input type="radio"/> 3 <input type="radio"/> 4 <input type="radio"/> 5	<input type="radio"/> 1 <input type="radio"/> 2 <input type="radio"/> 3 <input type="radio"/> 4 <input type="radio"/> 5
<p>Overall Quality Score Your subjective rating of the overall quality of the video, considering all factors above.</p>	<input type="radio"/> 1 <input type="radio"/> 2 <input type="radio"/> 3 <input type="radio"/> 4 <input type="radio"/> 5	<input type="radio"/> 1 <input type="radio"/> 2 <input type="radio"/> 3 <input type="radio"/> 4 <input type="radio"/> 5

Scale: 1 = lowest, 5 = highest

[Next](#)

Figure 8. User Study Interface. A screenshot of our web-based platform where participants evaluate video pairs based on temporal and spatial consistency.

PERSIST configurations consistently outperform the baselines in every head-to-head comparison. During head-to-head comparisons between PERSIST-S and PERSIST-XL, PERSIST-S narrowly wins on 3D Spatial Consistency (+0.21), while PERSIST-XL achieves a slightly higher Overall Quality Score (+0.14). The differences in Visual Fidelity and Temporal Consistency are too narrow to call for either side. While PERSIST-XL achieves a better FVD, the results of the study indicate that humans do not observe a significant performance degradation when we decrease the number of spatial tokens allotted to \mathcal{W}_θ . In contrast, PERSIST-XL+ w_0 wins most head-to-head comparisons against PERSIST-XL and PERSIST-S, which indicates that providing direct 3D conditioning generally improves performance.

Finally, users consistently prefer ground-truth videos across all metrics, highlighting that even our strongest configurations remain below the quality of real trajectories. This persistent gap underscores both the difficulty of long-horizon world modelling with procedurally generated environments, and the opportunity for further advances in persistent 3D generative representations.

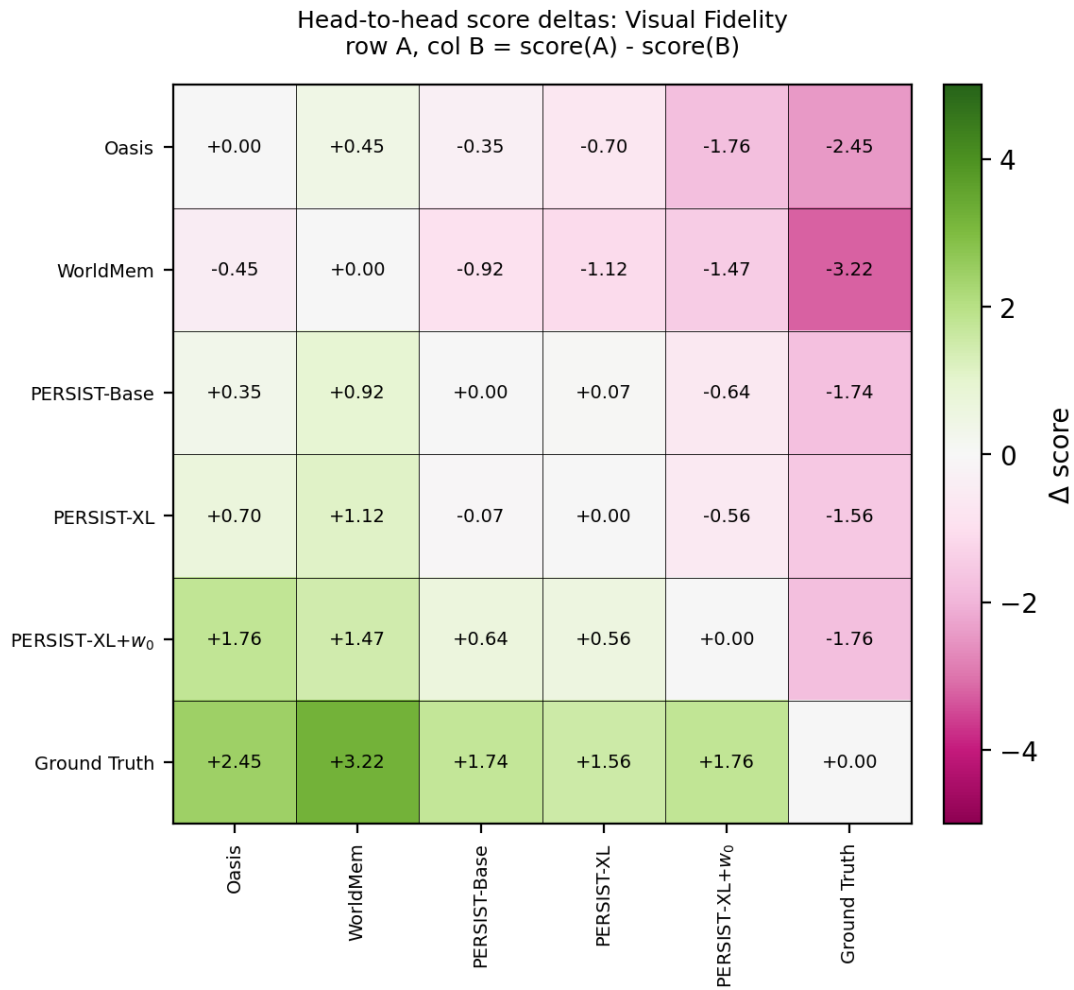


Figure 9. Score differences during head-to-head comparisons, **visual fidelity**.

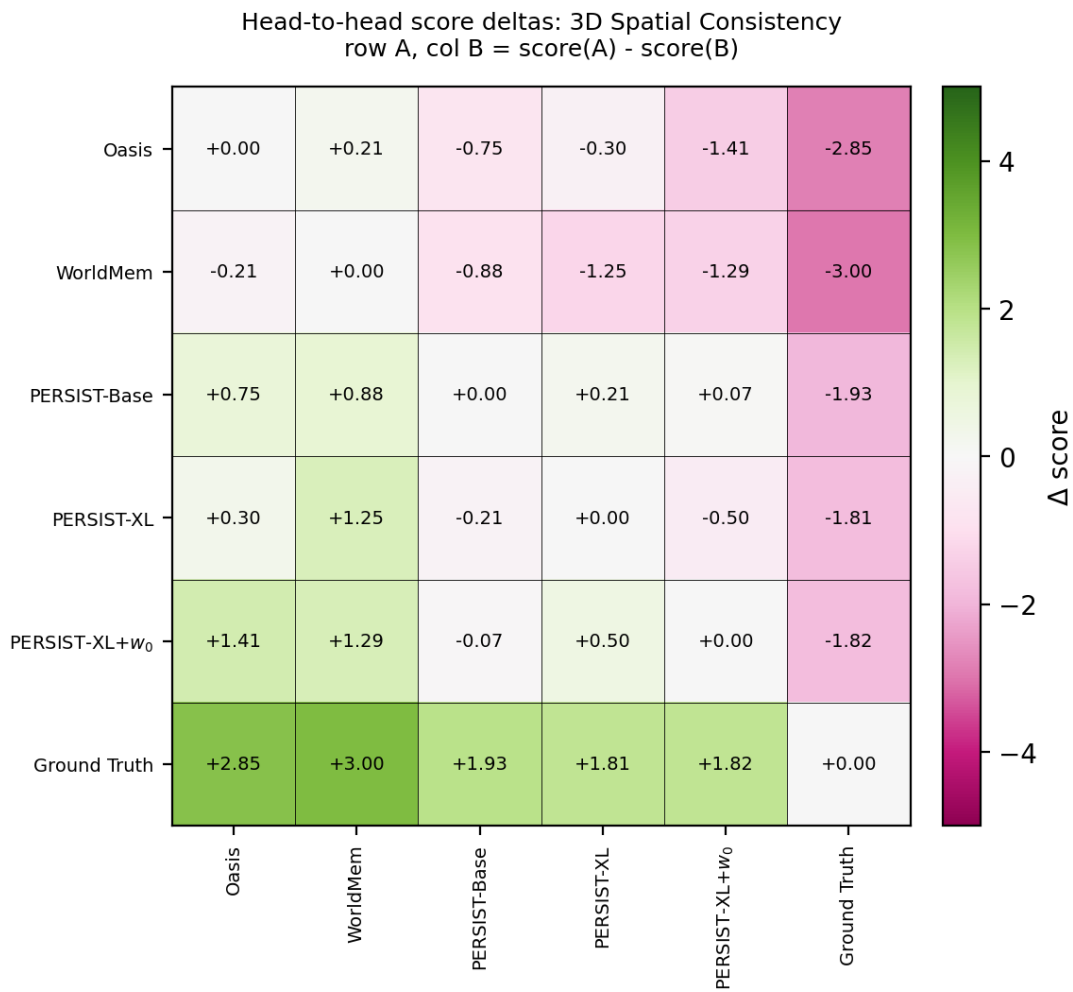


Figure 10. Score differences during head-to-head comparisons, **3D spatial consistency**.

Head-to-head score deltas: Temporal Environment Stability and Consistency
 row A, col B = score(A) - score(B)

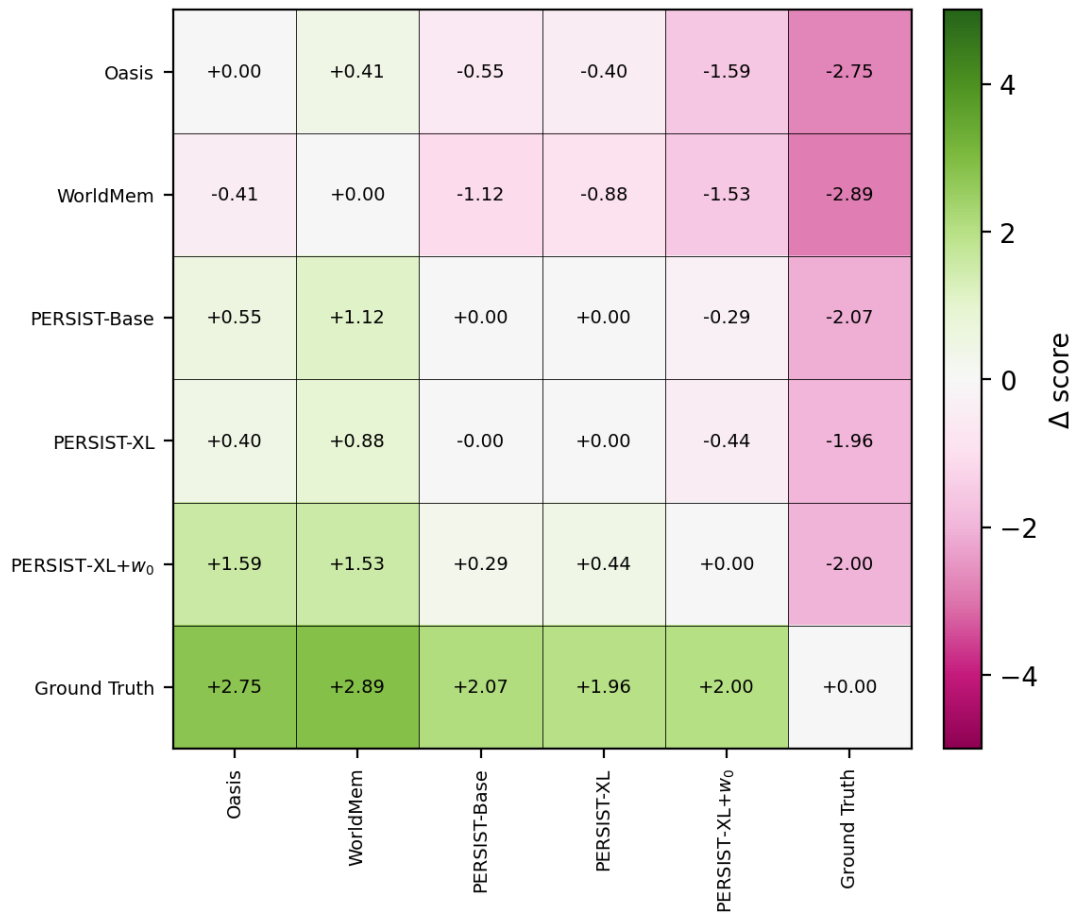


Figure 11. Score differences during head-to-head comparisons, **temporal consistency**.

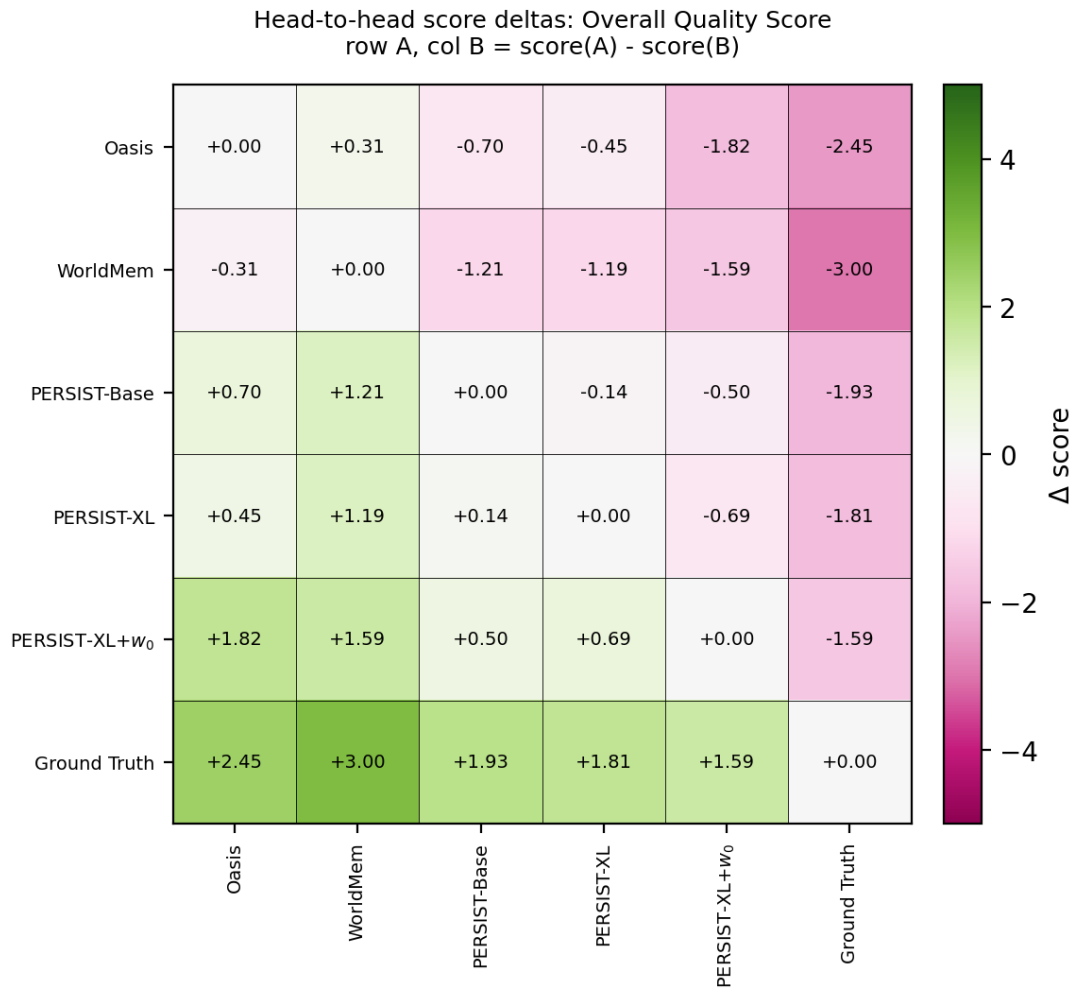


Figure 12. Score differences during head-to-head comparisons, **overall quality score**.

C.2. Scores for Each Evaluation Set

Table 9. Per set user study scores: **circle around**.

Method	Per Frame Visual Fidelity \uparrow	3D Consistency \uparrow	Temporal Consistency \uparrow	Overall Score \uparrow
Oasis	2 ± 0.2	1.6 ± 0.2	1.5 ± 0.2	1.6 ± 0.2
WorldMem	1.7 ± 0.2	1.5 ± 0.1	1.3 ± 0.1	1.4 ± 0.1
PERSIST-S	2.8 ± 0.2	2.6 ± 0.2	2.3 ± 0.2	2.5 ± 0.2
PERSIST-XL	3.0 ± 0.2	2.5 ± 0.1	2.2 ± 0.1	2.5 ± 0.1
PERSIST-XL $+w_0$	3.4 ± 0.2	3.0 ± 0.2	2.7 ± 0.3	3.1 ± 0.2

Table 10. Per set user study scores: **free play**.

Method	Per Frame Visual Fidelity \uparrow	3D Consistency \uparrow	Temporal Consistency \uparrow	Overall Score \uparrow
Oasis	2.3 ± 0.2	2.2 ± 0.2	2.0 ± 0.2	2.0 ± 0.2
WorldMem	1.5 ± 0.2	1.5 ± 0.2	1.2 ± 0.1	1.3 ± 0.1
PERSIST-S	3.0 ± 0.2	2.9 ± 0.2	2.8 ± 0.2	3.0 ± 0.2
PERSIST-XL	2.9 ± 0.2	2.8 ± 0.2	2.8 ± 0.2	2.8 ± 0.2
PERSIST-XL $+w_0$	3.6 ± 0.2	3.1 ± 0.2	3.3 ± 0.2	3.4 ± 0.2

Table 11. Per set user study scores: **backwards and look around**.

Method	Per Frame Visual Fidelity \uparrow	3D Consistency \uparrow	Temporal Consistency \uparrow	Overall Score \uparrow
Oasis	1.9 ± 0.2	2.0 ± 0.2	2.0 ± 0.2	1.9 ± 0.2
WorldMem	1.7 ± 0.2	1.8 ± 0.2	1.6 ± 0.2	1.6 ± 0.1
PERSIST-S	3.0 ± 0.2	2.7 ± 0.2	2.7 ± 0.2	2.6 ± 0.2
PERSIST-XL	2.7 ± 0.2	2.4 ± 0.2	2.4 ± 0.2	2.5 ± 0.1
PERSIST-XL $+w_0$	3.0 ± 0.2	2.6 ± 0.2	2.6 ± 0.2	2.8 ± 0.2

Table 12. Per set user study scores: **forward and look around**.

Method	Per Frame Visual Fidelity \uparrow	3D Consistency \uparrow	Temporal Consistency \uparrow	Overall Score \uparrow
Oasis	2.4 ± 0.2	2.0 ± 0.2	1.8 ± 0.2	1.9 ± 0.2
WorldMem	2.1 ± 0.2	2.2 ± 0.2	1.9 ± 0.2	1.9 ± 0.2
PERSIST-S	2.2 ± 0.2	2.3 ± 0.2	2.1 ± 0.2	2.3 ± 0.2
PERSIST-XL	2.6 ± 0.2	2.3 ± 0.2	2.3 ± 0.2	2.4 ± 0.1
PERSIST-XL $+w_0$	2.7 ± 0.2	2.4 ± 0.2	2.3 ± 0.2	2.4 ± 0.2

D. Limitations and Future Work

Training without ground truth 3D supervision. Our results underscore the critical role of explicit 3D representations in maintaining environmental coherence over long horizons. Currently, however, PERSIST acquires this representation via supervised training, restricting its applicability to simulators or datasets providing 3D annotations (e.g. Zhou et al., 2018; Chang et al., 2017; Yeshwanth et al., 2023). A key direction for future work is to relax this dependency by learning 3D representations directly from pixels, or by leveraging recent advances in 2D-to-3D foundation models (Wang et al., 2025; Team et al., 2025) to generate synthetic 3D annotations as a pre-processing step.

Eliminating exposure bias. While PERSIST yields substantial improvements in generation quality, temporal stability, and environmental coherence over baselines, human evaluators tend to prefer ground-truth videos in head-to-head comparisons, reporting a gradual degradation in visual quality and environment coherence over time. We attribute this degradation primarily to exposure bias: during training, individual pipeline components (\mathcal{W}_θ , \mathcal{C}_θ and \mathcal{P}_θ) are trained using ground truth data; at inference, they condition on their own past predictions and on predictions from other components, causing a train-inference distribution mismatch that grows over time. We report examples of generation glitches that occur over the course of a 2000 steps episode in Figure 14. Leveraging PERSIST’s fully differentiable pipeline, future work could explore incorporating an end-to-end post-training stage on generated rollouts, thereby aligning the training and inference distributions. As demonstrated in recent work (Huang et al., 2025c), this approach can be effective in making AR models robust to their own imperfect predictions.

Unconstrained spatial memory. PERSIST presently tracks a finite region of 3D space centred on the agent, causing information from distant locations to be discarded as the agent moves through the environment. To retain spatial information over arbitrarily large environments, future work could consider a conditioning strategy for \mathcal{W}_θ based on loading spatial chunks from a 3D memory bank. Whereas pixel memory banks suffer from viewpoint redundancy, a 3D store is inherently deduplicated and spatially organized, offering unique advantages for efficient storage and retrieval of spatial information.

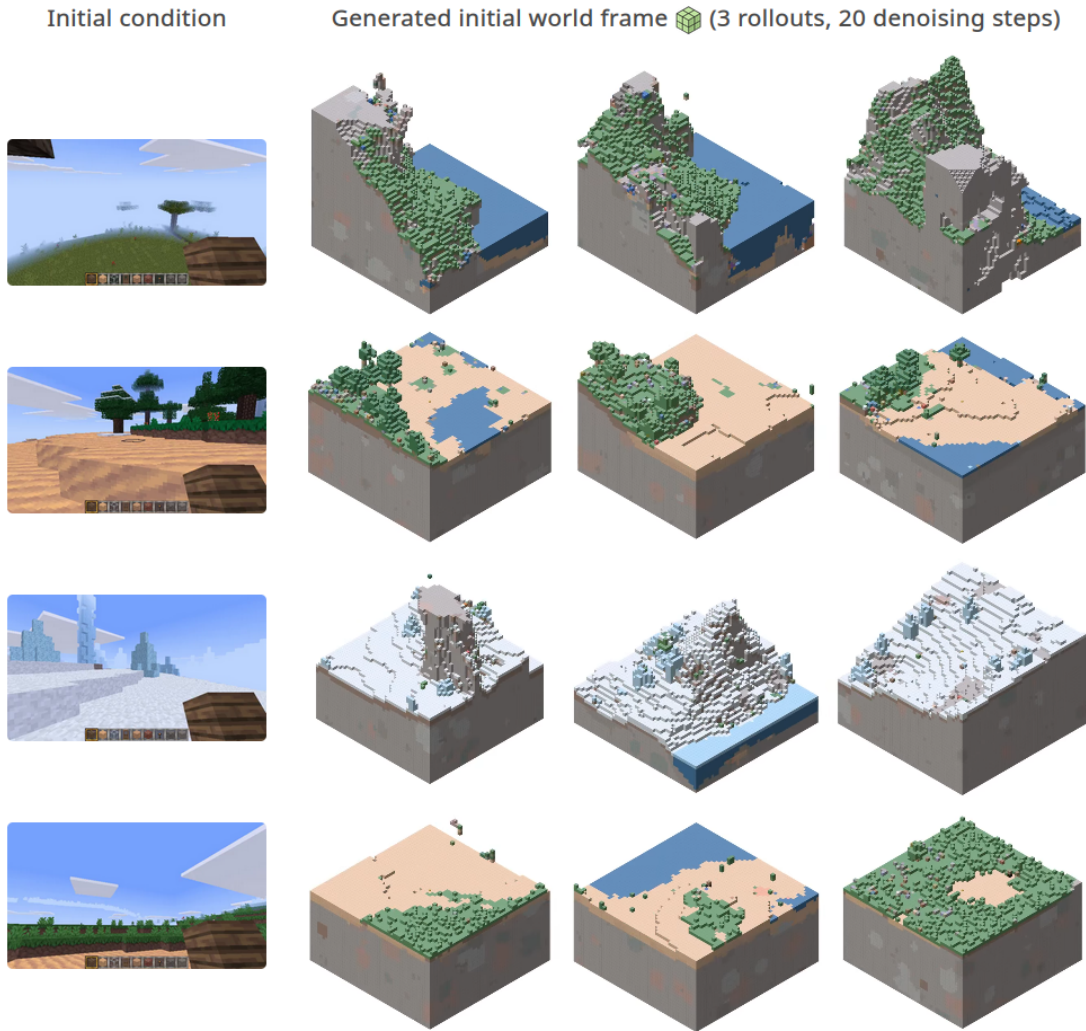


Figure 13. PERSIST generates diverse but coherent initial world frames from a single RGB conditioning observation. Each row corresponds to a specific input RGB frame, while each column depicts the initial world frame sampled from \mathcal{W}_θ during a specific generation episode.



Step 0 (0 seconds). Start of the episode. Generation is stable.



Step 672 (28 seconds). A tree trunk disappears from the 3D representation. As a result only the tree foliage is rendered to the left of the agent.



Step 888 (37 seconds). Several wood blocs are wrongly predicted by \mathcal{W}_θ and appear in the 3D representation. They get rendered in the agent's view.



Step 1296 (54 seconds). The texture of the ground is drifting to a yellowish colour. The 3D representation remains stable.



Step 1320 (55 seconds). \mathcal{P}_θ recovers the correct texture thanks to the grounding provided by w_{2D} .



Step 1656 (69 seconds). A collision gets mispredicted and the agent clips through a bloc. The ground texture begins to drift.



Step 1680 (70 seconds). The model recovers from terrain clipping and texture drift after the agent executes a jump action.



Step 2000 (83 seconds). The episode concludes on a stable frame. The environment remains globally coherent after 2000 steps, but glitches occur more frequently due to exposure bias.

Figure 14. Generation glitches and subsequent recoveries over a 2000 step (83 seconds) episode generated with PERSIST. The 3D representation drifts locally, causing individual blocs to appear and disappear from the agent's view. However we find that the 3D representation remains globally coherent and has a net stabilising effect on generation, allowing \mathcal{P}_θ to recover from visual artifacts. This lets PERSIST generate rollouts lasting thousands of steps, even if glitches become more frequent over time due to autoregressive drift.